

Tethered hard spheres: A bridge between the fluid and solid phases

James MacKinnon,¹ Marcus N. Bannerman,² and Leo Lue^{1, a)}

¹⁾*Department of Chemical and Process Engineering, University of Strathclyde, James Weir Building, 75 Montrose Street, Glasgow G1 1XJ, United Kingdom*

²⁾*School of Engineering, University of Aberdeen, Aberdeen, AB24 3UE, United Kingdom*

(Dated: 17 August 2022)

The thermodynamics of hard spheres tethered to a Face-Centered Cubic (FCC) lattice is investigated using event-driven molecular-dynamics. The particle-particle and the particle-tether collision rates are related to the phase space geometry and are used to study the FCC and fluid states. In tethered systems, the entropy can be determined by at least two routes: (i) through integration of the tether collision rates with the tether length r_T or (ii) through integration of the particle-particle collision rates with the hard-sphere diameter σ (or, equivalently, the density). If the entropy were an entirely analytic function of r_T and σ , these two methods for calculating the entropy should lead to the same results; however, a non-analytic region exists as an extension of the solid-fluid phase transition of the untethered hard-sphere system, and integration paths that cross this region will lead to values for the entropy that depend on the particular path chosen. The difference between the calculated entropies appears to be related to the comunal entropy, and the location of the non-analytic region appears to be related to conditions where the regions of phase space associated with the FCC configuration become separated from those associated with the disordered fluid. The non-analytic region is finite in extent, vanishing below $r_T/a \approx 0.55$, where a is the lattice spacing, and there are many continuous paths that connect the fluid and solid phases that can be used to determine the crystal free energy with respect to the fluid.

I. INTRODUCTION

The hard-sphere system is a foundational thermodynamic model; providing the first example of a purely-entropic transition from the disordered fluid phase to an ordered solid crystalline phase¹. Determining the location of this transition is not trivial, as these two phases are separated by a strong first-order phase transition that cannot be avoided; as a result, straightforward thermodynamic integration cannot be used to calculate the free energy difference between the phases, due to the presence of hysteresis². As a consequence, different methods need to be developed. Hoover and Ree³ introduced the single occupancy model to more precisely explore the hard-sphere fluid-solid transition. In this model, space is partitioned into mutually exclusive regions, such as the Voronoi polyhedra constructed from an FCC lattice, and the centers of the particles are constrained to remain in one of these regions. This model was employed by Woodcock^{4,5} to finally establish that FCC lattices are marginally more stable than hexagonal close packed (HCP), a remarkable achievement at the time. Meanwhile, Speedy⁶ had proposed in 1993 a closely related model where each of the particles were “tethered” to remain within a set distance from a location in the system, rather than confined to disjoint regions of space. This approach was explored for non-spherical particles by Donev and co-workers⁷ in 2007 although their analysis is restricted to the close-packed limit. The tethered particle model was recently reanalyzed in 2021 from the perspective of phase space allowing the development of additional methods to calculate the free energy without considerable restriction, including even in the fluid phase⁸. These approaches are easily generalized to arbitrary dimensions and have already been used to determine the free energy of various crystal structures of hard hy-

perspheres in six dimensions⁹. It is remarkable that, despite 65 years of simulation, the hard-sphere model continues to provide insight into phase transitions, and it still remains a rich testing ground for developing new free-energy sampling techniques.

The tethered hard-sphere model has frequently only been used as a means to determine the free energy of the untethered hard-sphere system; however, this work considers the thermodynamics of the tethered hard-sphere model on its own merits to gain insight into the structure of phase space for hard-sphere systems. This additional insight is possible as the tether collision rate is directly related to the geometry of the configurational phase space⁸ and thus to the entropy and the free energy of the system. As a result of this analysis, we also aim to provide general guidelines for finding and using continuous paths between the solid and fluid phases for determining the free energy of solids.

The remainder of this paper is organized as follows. In the next section, the tethered hard sphere model is briefly described and the details of the molecular dynamics simulations are provided. Afterwards, the data for the particle-particle and the tether collision rates from the simulations are presented and reviewed. Then, in Sec. IV, the consistency of these data is examined and then used to determine the entropy of the system. With knowledge of the entropy and the collision rates, the geometry of the accessible phase of tethered hard sphere systems examined in Sec. V. In Sec. VI, a diagram of states is presented for the tethered hard sphere model, which includes a discussion of the properties of the system in each of these states. Finally, the main findings of the paper are summarized in Sec. VII, along directions for future research.

^{a)}Electronic mail: leo.lue@strath.ac.uk

II. SIMULATION DETAILS

The system studied here is comprised of $N = 13500$ particles in a cubic periodic volume V , which is varied in size to control the number density $\rho = N/V$. The particles are identical and have a diameter σ and mass m . Each is restricted to remain within a distance r_T from a ‘‘tether’’ point. While the tether point can be located arbitrarily, in this study the tether point is an FCC (face centered cubic) lattice site to generate pathways from the most-stable hard-sphere crystal state. To generate measurements of this system, event-driven molecular dynamics (EDMD) simulations are performed using DynamO¹⁰. For each state point, three configurations of spheres are initialized in a perfect FCC lattice. The velocities are randomly assigned from a Maxwell-Boltzmann distribution and then shifted and rescaled to zero the total momentum of the systems and to set the kinetic temperature exactly equal to one. An Andersen thermostat is used to thermalize the system, as ergodicity is poor at short tether lengths⁸, and its mean-free time is adjusted to set it to 5% of the total number of events. The Andersen thermostat is adjusted every 100 N events and is typically stable after the first adjustment.

Each configuration is first equilibrated for $10^3 N$ events before ten production runs of $10^3 N$ events are performed to collect averages. Measurement uncertainties are estimated by taking the standard deviation of results from the three configurations and each of their ten production runs. All results are reported in reduced units using the particle diameter σ as a length scale, particle mass m as the mass scale, and temperature to provide the time scale $\sqrt{m\sigma/(k_B T)}$. The key dimensionless parameters of the system are the reduced density $\rho\sigma^3$ and the reduced tether length r_T/σ ; however, it is more convenient to consider the tether length reduced by distance between nearest FCC tether points, $a/\sigma = (\rho_c/\rho)^{1/3}$, where $\rho_c\sigma^3 = \sqrt{2}$ is the close-packed number density for the FCC lattice.

III. EVENT RATES

In this section, the rates of particle-particle collisions and tether events from the EDMD simulations are analyzed. As shown previously⁸, the tether event rates are directly related to the geometry of the accessible configurational phase space of the hard sphere system. This is briefly summarized here.

Consider the tethered hard sphere system as a single state point moving through a $3N$ -dimensional vector space, which is the configurational phase space of the system. As overlaps are not possible in this system, the configurations where pairs of spheres intersect create impenetrable walls within the configurational phase space which the system state point cannot enter. The ‘‘thickness’’ of these walls is directly related to the hard-sphere diameter. The state point bounces off these walls continuously as each intersection with these walls is a particle-particle collision. Ergodicity is typically assumed, thus the state point is assumed to visit phase space evenly. This ultimately implies that the geometry of this phase space, including measures such as the surface-to-volume ratio, are directly

related to the rates of particle-particle events, and thus to pressure and other thermodynamic variables. The configurational phase space is considered to be ‘‘unravell’d’’, so that it extends infinitely in all dimensions. Thus, the periodic boundary conditions imposed on the simulations cause these particle-particle walls associated with the excluded volume interactions to repeat throughout the vector space.

With this background it is interesting to contrast the effect of the tethers. The tethers confine the system state point to remain within a fixed region in phase space. Geometrically, this region corresponds to a hyperdimensional volume formed by a union of N three-dimensional spheres each sited on the lattice site of a particle in its coordinates only and with a radius of the tether length, thus it is a highly localised volume in phase space. Again the tether collision rates are directly related to how much of the confining tether hypersurface is accessible to the state point particle compared to the hypervolume of the accessible space. Crucially though, the geometry of the tether volume is known, thus measurements of the tether event rate can be used to determine the hypersurface area. As this can only be reduced by particle-particle walls intruding into the tethered region, the tether rates can indirectly tell us about that geometry too. With this established, it is interesting to examine the rate of tether collisions and how it varies in the FCC tethered hard-sphere system.

The ideal tether model is a system where the particles only collide with their tethers; there are no particle-particle collisions. This corresponds to systems with tethers such that

$$\frac{r_T}{a} \leq \max\left(0, \frac{1}{2}\left(1 - \frac{\sigma}{a}\right)\right) = \max\left(0, \frac{1}{2}\left(1 - \left(\frac{\rho}{\rho_c}\right)^{1/3}\right)\right), \quad (1)$$

so that the particles are unable to interact with each other. For the ideal tether model, the tether collision rate \mathcal{N}_T is given by⁸

$$\mathcal{N}_T^{\text{id}} = (2\pi\beta m)^{-1/2} N \frac{D}{r_T}, \quad (2)$$

where $D = 3$ is the dimensionality of the system, $\beta = 1/(k_B T)$, k_B is the Boltzmann constant, and T is the absolute temperature of the system. Generally, the observed tether rate is reduced below this ideal tether model as the particle-particle walls in phase space reduce the accessible area of the tether volume; however, values above it have been observed at high densities where the accessible hypervolume has been reduced sufficiently to offset reductions in the hypersurface area as shown later.

The particle-particle collision rate $\dot{\mathcal{N}}$ is directly related^{11,12} to the pressure p of the system as follows,

$$\frac{\beta p}{\rho} = 1 + (\pi\beta m\sigma^2)^{1/2} \frac{\dot{\mathcal{N}}}{DN}. \quad (3)$$

As a basis for comparison, the pressure of hard sphere systems in the fluid phase is well described by the Carnahan-Starling

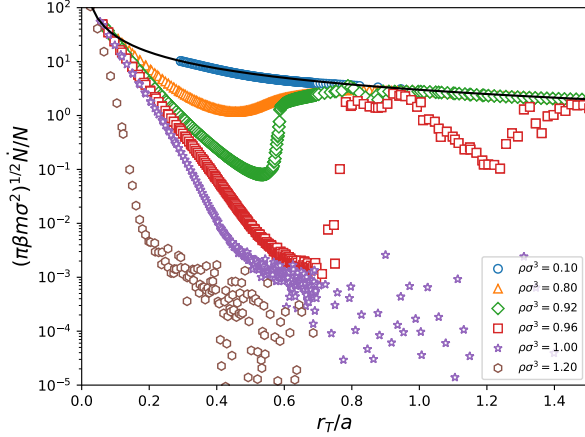


FIG. 1. Variation of the tether collision rates with the tether length for systems of hard spheres tethered to an FCC lattice at different densities in the fluid phase. The solid black line is the tether collision rate for the ideal tether model (see Eq. (2)).

equation of state¹³.

$$\frac{\beta p}{\rho} = 1 + \frac{4y(1-y/2)}{(1-y)^3} \quad (4)$$

where $y = \pi\rho\sigma^3/6$ is the volume fraction of space occupied by the spheres. For the solid phase, the equation of state from Pieprzyk and coworkers¹⁴ is used for comparison,

$$\frac{\beta p}{\rho} - 1 = \frac{3}{1-\omega} + Ae^{B(1-\omega)} + Ce^{D(1-\omega)} - E \quad (5)$$

where $A = 0.01622$, $B = 6.151$, $C = 3.8437 \times 10^{-5}$, $D = 27.72$, $E = 0.49541$, and $\omega = \rho/\rho_c$.

The tether and particle-particle event rates for *tethered* system over a range of densities and tether lengths are shown in Fig. 1 and Fig. 2. Care must be taken to not label the tethered system as a fluid at any point as it always contains some long-range order; however, as it is an extension of the untethered system it is natural to explore representative densities in the untethered fluid ($\rho\sigma^3 = [0.1, 0.8, 0.92]$), solid ($\rho\sigma^3 = [1.0, 1.2]$), and transition ($\rho\sigma^3 = 0.96$) densities. Generally, tether event rates decrease with increasing tether length, which may be expected as the confining tether hyper-surface area to accessible volume ratio decreases, which is the source of the $1/r_T$ scaling in the ideal tether rate (see Eq. (2)). All densities in the fluid range display a dip below the ideal tether rate as particle-particle interactions begin to occur, but approach the ideal rate once the tether radius is large enough ($r_T/a \gtrsim 1$). At this point the tethered system can access the majority of the configurations contributing to the pressure and it can be seen in Fig. 2 that the particle-particle collision rates approach a value very closely predicted by the Carnahan-Starling equation of state for hard sphere fluids (by combining Eqs. (4) and (3)). It can be imagined that, once particles can

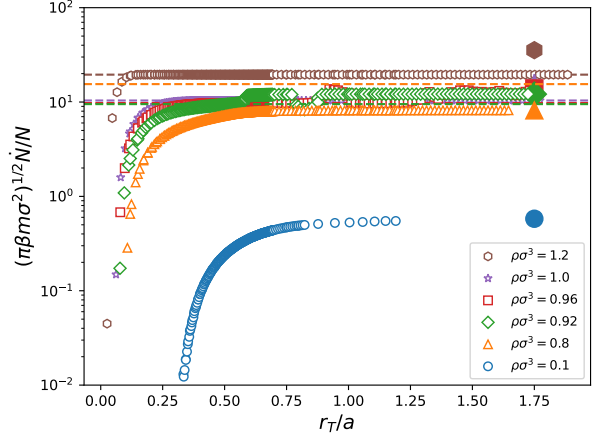


FIG. 2. Variation of the particle-particle collision rates with the tether length for systems of hard spheres tethered to an FCC lattice at different densities in the fluid phase. The small symbols denote particle-particle collision measurements, while the larger corresponding symbol indicates the particle-particle collision rates predicted from the Carnahan-Starling equation of state for the fluid phase (see Eq. (4)). The dashed lines represent the particle-particle collision rates predicted from the equation of state of Pieprzyk and coworkers¹⁴ for the solid phase.

fully interact with their neighbors at $r_T/a \approx 1$, the remaining configurations are either translations of already accessible configurations, or large density fluctuations which are improbable in this system, thus phase space begin to takes on a regular structure, which is analyzed in more depth later (e.g., see Fig. 7).

For solid densities, the tether event rates in Fig. 1 again decrease as tether length is increased; however, unlike in the fluid density range, there is no increase back to the ideal tether rate line, where the event rates appear to level off at a value close to zero temporarily before dropping off the figure to zero. The system appears to be localized in phase space by the particle-particle “walls” and unable to reach the tether surface, which becomes a redundant confinement for long tethers. Its clear in Fig. 1 that particles rarely travel further than $r_T/a \approx 0.75$. The particle collision event rates in Fig. 2 for solid densities also show an increase initially with increasing tether length as in fluid densities, before quickly levelling off at a value very closely predicted by the Pieprzyk equation of state for hard sphere fluids (by combining Eqs. (5) and (3)), denoted by the horizontal dashed lines in the figures.

Finally, the density $\rho\sigma^3 = 0.96$ is considered as it lies within the fluid-solid transition density for the untethered system, from the onset of freezing $\rho_f\sigma^3 \approx 0.93890$ to the melting density $\rho_s\sigma^3 \approx 1.03715$ ⁸. This density in particular is chosen as there is a clear minimum in the tether collision rate with tether length for densities up to $\rho\sigma^3 \approx 0.96$ before they “melt” at longer tether lengths ($r_T/a \gtrsim 0.5$) to the ideal tether model suggesting that the tethered “fluid” is recovered. At higher densities, this minimum continues to deepen; how-

ever, the collision rate no-longer increases back up to the ideal tether collision line, as for the density $\rho\sigma^3 \approx 1.0$ in Fig. 1. This can be interpreted to mean that the system remains in the solid phase and does not quite “escape” from the solid phase to transition to a liquid, although this cannot be precisely defined as the system may yet still melt at longer tether lengths or simulation times than studied here.

Consider again the particle collision rates in Fig. 2 and the result for the same transition density $\rho\sigma^3 \approx 0.96$ and the adjacent densities. For $\rho\sigma^3 < 0.91$, the particle collision rates clearly trend towards and level off at the values predicted by the Carnahan-Starling equation of state, indicating that these systems closely model fluids. For $\rho\sigma^3 > 0.97$, the particle collision rates clearly trend towards and level off at the values predicted by the Pieprzyk equation of state, indicating that these systems closely model solid hard sphere systems; however, at values of $0.91 < \rho\sigma^3 < 0.97$, the trend towards the equation of state predictions is far less clear and the highlighted curve at $\rho\sigma^3 = 0.96$ shows this clearly, where the initial trend with increasing tether looks to be towards the solid equation of state line, before there is a sharp increase in collision rate up to the fluid equation of state prediction, and then another “jump” back and forth, presumably between the two phases. The tether lengths that these jumps happen at match up with those where the minimum in tether collision rates are observed (see Fig. 1). This further emphasizes that the system is seemingly becoming jammed and unjammed as the tether length is made longer through densities around this transition region. This suggests there is “jumping” between phases as the system is forced into different configurations which each allow more or less freedom of movement. It is clear that a transition region exists in the tether space as well as the density space thus a phase diagram might be considered provided the free energy can be calculated, and this is discussed in the following section.

IV. CALCULATION OF THE ENTROPY

As discussed earlier and in our previous work⁸, the event rates in this system are directly related to ratio of the exposed surface area associated with the event and the volume of accessible phase space. The entropy S is directly related to the tether collision rate and the particle-particle collision rate,

$$\begin{aligned} k_B^{-1} dS &= d \ln \Omega_T(\rho, r_T, \sigma) \\ &= (\pi\beta m)^{1/2} \left(\dot{N}_T a \sqrt{2} d \left(\frac{r_T}{a} \right) - \frac{\sigma}{D} \dot{N} \frac{d(\rho\sigma)^D}{\rho\sigma^D} \right), \quad (6) \end{aligned}$$

where Ω_T is the density of states and D is the dimensionality. This relation provides at least two routes to calculate the entropy of the tether system⁸. The first is to integrate the particle-particle collision rate with respect to the density and hard-sphere diameter σ , while holding the tether length con-

stant,

$$\begin{aligned} \Delta S_T^{(\sigma)}/k_B &= \ln \frac{\Omega_T(\rho, r_T, \sigma)}{\Omega_T^{\text{id}}(r_T)} \\ &= -\frac{1}{D} \int_{\rho_0}^{\rho} \frac{d(\rho'\sigma^D)}{\rho'\sigma^D} (\pi\beta m\sigma^2)^{1/2} \dot{N}. \quad (7) \end{aligned}$$

The excess entropy calculated using this expression $\Delta S_T^{(\sigma)}/k_B$ corresponds to standard thermodynamic integration.

The other path is to integrate the tether collision rate with respect to the tether length, while holding the density and hard-sphere diameter constant. The entropy difference between a tethered system and an ideal tethered system at the same tether length and particle density can be determined from the tether event rate \dot{N}_T as:

$$\begin{aligned} \Delta S_T^{(r_T)}/k_B &= \ln \frac{\Omega_T(\rho, r_T, \sigma)}{\Omega_T^{\text{id}}(r_T)} \\ &= \int_{r_{T,0}}^{r_T} dr'_T (2\pi\beta m)^{1/2} \dot{N}_T^{\text{id}} \left(\frac{\dot{N}_T}{\dot{N}_T^{\text{id}}} - 1 \right) \\ &= D \int_{r_{T,0}}^{r_T} \frac{dr'_T}{r'_T} \left(\frac{\dot{N}_T}{\dot{N}_T^{\text{id}}} - 1 \right). \quad (8) \end{aligned}$$

The excess entropy calculated using this expression is known as the tether integration route. The difference between the entropy of the tethered hard sphere system and that of an ideal tethered system at the same density and tether length is deemed the “excess” entropy (i.e. $\Delta S_T(\rho, r_T, \sigma) \equiv S_T(\rho, r_T, \sigma) - S_T^{\text{id}}(r_T)$). The excess entropy estimated using the two different methods presented above is shown in Fig. 3. If the entropy is an analytic function for all densities and tether lengths, the two methods of calculating the entropy should lead to the same results. This is generally true at low densities and tether lengths; however, the two routes diverge in the range of densities between the freezing and melting densities at longer tether lengths.

To better understand this difference, it is illuminating to compare the calculated *excess* entropies against theoretical predictions for the *residual* entropy of the untethered hard sphere system⁸. The residual entropy is defined as the difference between the entropy of a system and the entropy of an ideal gas with the same number of particles, volume, and temperature. The excess tethered entropy is expected to approach the residual untethered entropy in the limit of long tethers,

$$\begin{aligned} S^{\text{res}}(\rho, \sigma) &= \lim_{r_T \rightarrow \infty} \Delta S_T(\rho, \sigma, r_T) \\ \ln \frac{\Omega(\rho, \sigma)}{\Omega^{\text{ig}}(\rho)} &= \lim_{r_T \rightarrow \infty} \ln \frac{\Omega_T(\rho, \sigma, r_T)}{\Omega_T^{\text{id}}(r_T)}. \quad (9) \end{aligned}$$

At densities below the hard sphere freezing density, the excess entropy of the tethered systems, calculated using both methods, lies below the residual entropies of the hard sphere system. This is expected as the tethered system is close to the maximally-spaced-out state, thus reducing the possibility

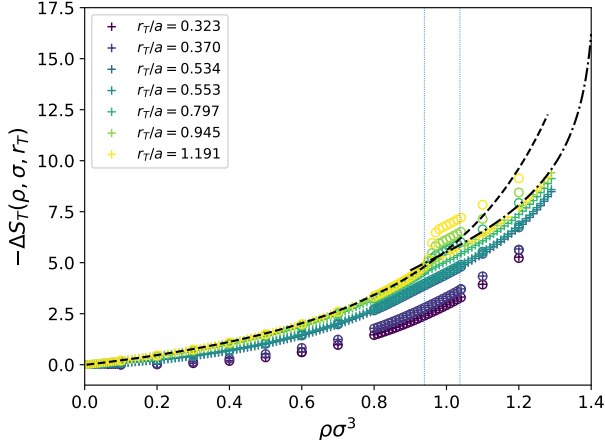


FIG. 3. The entropy of the tethered hard sphere model over a range of conditions. The crosses are the result of numerical integration of the particle-particle collision rate data with respect to density (or, equivalently, hard sphere diameter) at fixed tether length ($\Delta S_T^{(\sigma)}/k_B$), using Eq. (7). The circles are the result of integration of the tether event rates with respect to the tether length using Eq. (8) at constant density and hard sphere diameter ($\Delta S_T^{(r_T)}/k_B$). The black dashed line is the residual free energy of the untethered hard sphere system in the fluid phase¹³, and the black dashed-dotted line is residual free energy in the solid phase¹⁴. The dotted vertical lines indicate the transition densities for the untethered hard-sphere system.

of interactions over an unconstrained state. The excess entropies gradually increase with the tether length and closely approach the residual entropy of the untethered hard-sphere fluid. Above the freezing density, calculated $\Delta S_T^{(\sigma)}/k_B$ values lie below the residual free energy of the hard sphere FCC solid (black dashed-dotted line); as tether length increases, the excess entropy approaches the residual entropy, just as before; however, calculated $\Delta S_T^{(r_T)}/k_B$ values lie above the residual free energy of the untethered hard-sphere solid.

Above the melting density, the tether collision rate drops rapidly with tether length (see Fig. 1). This is an indication that the system becomes trapped in the region of phase space around the perfect FCC lattice by the excluded volume interactions. In this situation, it could be expected that the excess entropy will continue to decrease without bound as the tether length increases. The volume of phase space accessible by the system remains constant as the tether length increases, while the phase space volume accessible to the ideal tether system continues to grow. In fact, if $\Delta S_T^{(r_T)}/k_B$ is shifted by the difference in the entropy between the ideal gas and ideal tether systems,

$$\ln \frac{\Omega_T^{\text{id}}(r_T)}{\Omega_T^{\text{ig}}(\rho)} = \ln \phi_T + \ln \frac{N!^{1/N}}{N}, \quad (10)$$

then the results are once again in close agreement with the residual entropy of the untethered systems, as shown in Fig. 4.

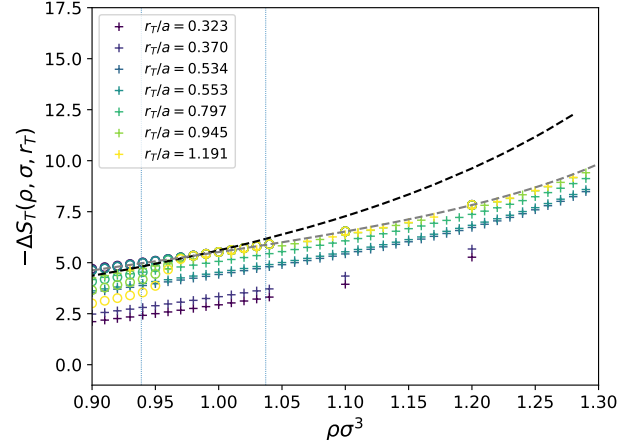


FIG. 4. The excess entropy of the tethered hard sphere model over a range of conditions. The crosses are the results for $\Delta S_T^{(\sigma)}/k_B$ while the circles are the results for $\Delta S_T^{(r_T)}/k_B$ plus the communal entropy difference constant. The dashed lines are the residual free energy of the untethered hard sphere system in the fluid phase¹³ (black) and the solid phase¹⁴ (grey). The dashed vertical lines indicate the transition densities for the untethered hard-sphere system.

In contrast, when $\Delta S_T^{(\sigma)}$ is shifted by $\ln \Omega_T^{\text{id}}(r_T)/\Omega_T^{\text{ig}}(\rho)$, the results move further from the residual entropies of the untethered systems for systems with longer tether lengths. This does not make physical sense, as the longer the tether length, the closer the system should resemble an untethered system. For the shorter tether lengths, these values, much like the shifted values from the tether integrations, also are in close agreement with the residuals of the untethered system.

Another manner to check the consistency of the data is to compare the pressure, as determined from the free energy obtained from tether event rates. The particle-particle collision rate for tethered systems is shown in Fig. 5. The crosses are directly from the EDMD simulations. The circles are calculated from derivatives of spline fits to the free energies calculated from tether integrations.

The collision rates derived from the integration of the tether event rates are in good agreement with the simulation data, with the exception of systems with sufficiently long tethers in and near the fluid-solid coexistence region. The fact that the pressures agree outside this region implies that the free energies from tether collision rate integration and the particle-particle collision rate integration are the same with respect to density, but are only shifted by a constant.

Figure 6 shows the difference between the excess entropies calculated via the two different methods. The difference is only non zero at densities lying in the solid phase for tether lengths of $r_T/a > 0.7$. There is a critical tether length $r_T/a \approx 0.55$ below which the entropies calculated using both methods are consistent across all densities. One key thing to note is that the difference between the entropies is dependent only on the tether length and not on the density. This observation is consistent with the fact that the pressures from the two

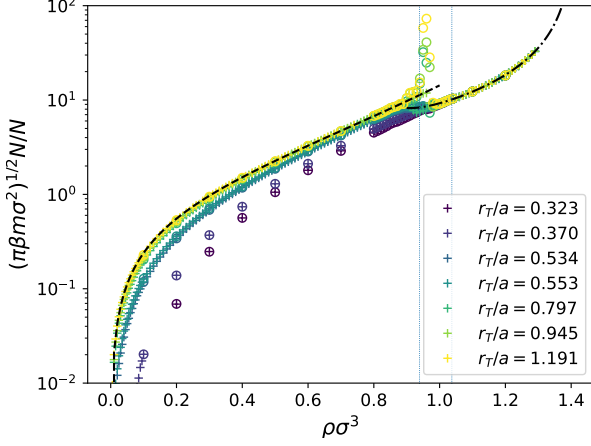


FIG. 5. The particle-particle collision rates of the tethered hard sphere model. The crosses are the data from the MD simulations, and the open circles are from the density derivatives of $\Delta S_T^{(r_T)}/k_B$, the entropy calculated via integration of the tether event rate. The black dashed line is the Carnahan-Starling¹³ equation of state, while the black dashed-dotted line is the equation of state developed by Pieprzyk and coworkers¹⁴ for the solid FCC phase.

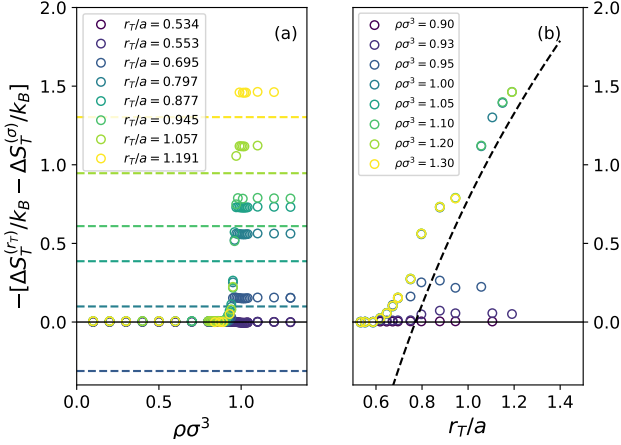


FIG. 6. The difference between $\Delta S_T^{(r_T)}/k_B$ (see Eq. (8)) and $\Delta S_T^{(\sigma)}/k_B$ (see Eq. (7)) (a) as a function of density for various tether lengths r_T/a , and (b) as a function of tether radius for various densities $\rho\sigma^3$.

routes are the same outside the transition region.

V. PHASE SPACE GEOMETRY

The event rates allow us to more carefully explore the geometry of phase space. For a tethered system, the maximum possible accessible volume is that of an ideal system (i.e. $\Omega^{\text{id}} = (4\pi r_T^3/3)^N$). The inclusion of excluded volume

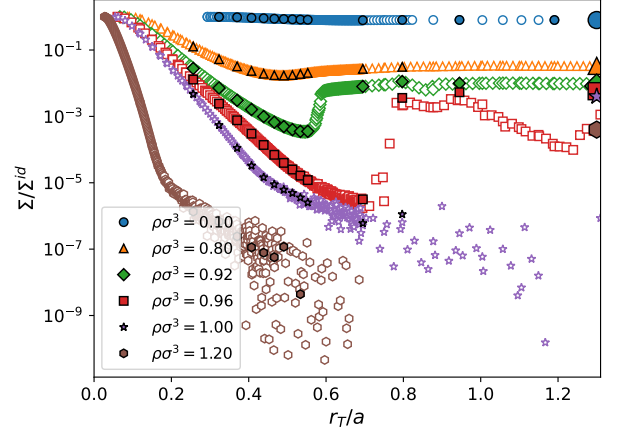


FIG. 7. Fraction of the tether surface area accessible by the tethered hard sphere system. Small empty symbols denote values calculated from particle collision integration, and small filled symbols (with a black outline) denote values from tether collision integration. The larger symbols on the right limit are used to denote the accessible phase space volume ratio in the untethered system.

between the particles will decrease the accessible volume of phase space and increase the bounding surface area. As the hard-sphere diameter increases, the thickness of these bodies will increase. There are two types of bounding surfaces: One corresponding to the tethers and the other corresponding to the particle excluded volumes (the constraint that particles cannot overlap). The tether collision rates are directly related to the area Σ of bounding surface due to the volume of phase space accessible by the system⁸ as given here,

$$\frac{\Sigma}{\Omega} = (2\pi\beta m)^{1/2} \dot{N}_T. \quad (11)$$

Let us first consider systems with a fixed tether length r_T/a and observe what happens with increasing the value of σ/a . In this case, the maximum available surface area will be constant and equal to the surface area in the ideal tether model. The fraction of the surface area in the ideal tether model that is accessible by the system can be determined by

$$\begin{aligned} \frac{\Sigma}{\Sigma^{\text{id}}} &= \frac{\dot{N}_T}{\dot{N}_T^{\text{id}}} \frac{\Omega_T(\rho, r_T, \sigma)}{\Omega_T^{\text{id}}(r_T)} \\ &= (2\pi\beta m)^{1/2} r_T \frac{\dot{N}_T}{ND} e^{\Delta S_T(\rho, r_T, \sigma)}. \end{aligned} \quad (12)$$

In Fig. 7, the fraction of the tether boundary which is accessible to the system as a function of tether length and density is presented. At fluid-like/low densities and large tether lengths, the fraction of the accessible surface area approaches a constant equal to the ratio of the volume of accessible phase space to that of an ideal tether system (i.e. $\Omega_T(\rho, r_T, \sigma)/\Omega_T^{\text{id}}(r_T)$). This can be rationalized by consider-

ing the phase space of the tethered hard sphere system to be a porous material, with the allowed regions corresponding to the pores of the system and the regions of phase space disallowed by the excluded volume and tether constraint corresponding to the pore walls. For a sufficiently large sample of a uniform porous material, the pore area fraction on an exposed surface is expected to be the same as the pore volume fraction in the bulk of the material, regardless of dimensionality.

At densities well above the freezing point, the ratio of the accessible surface area in in Fig. 7 no longer approaches the ratio of the accessible phase space volume at large tether lengths but instead it falls to values far below it. At these solid densities, the system is locked into a small section of phase space by the particle-particle excluded volume interactions, and there is almost no possibility of reaching the tether bound phase space boundary. Finally, consider the fraction of accessible tether bound surface area for the density in the transition region. There is a clear minimum observed in the data, similar to that observed in the tether collision rate data for lower densities; however, the area does not recover to the untethered limit and appears to show considerable instability over the tether lengths considered.

The data for tether collisions and accessible surface area suggest that as the tether length initially increases, particle-particle collisions block the system from reaching the tether surface, which means that the pathways for the system to escape the FCC region of phase space become restricted. As the tether length is increased beyond a certain value, the fraction of accessible tether bound surface area increases, which means that pathways out of the FCC configuration widen. This decrease and subsequent increase of $\Sigma/\Sigma^{\text{id}}$ with tether length suggests that there is a ‘‘bottleneck’’ in the pathways from the region of phase space near the perfect FCC configuration and that of the disordered fluid. At these transition densities, the particle-particle interactions seem to form a distinct barrier that distinguishes these regions of phase space from each other.

Figure 8 shows the variation of the accessible ratio of tether bound phase space area with increasing density. This can be pictured as a study of how a fixed region of phase space bound by the tether constraints becomes increasingly inaccessible by the system as the hard sphere diameter is increased. The ratio $\Sigma/\Sigma^{\text{id}} = 1$ when $\rho\sigma^3 = 0$ and decreases monotonically with increasing for the ratio of accessible surface area as particle diameter for all tether volumes used. The rate of decrease with density increases as the tether length increases. At very short tether lengths, the presence of excluded volume interactions do not significantly decrease the accessible surface area until the density becomes fairly large; this is, in part, due to the fact that the FCC configuration is the most efficiently packed. For very long tether lengths, the rate of drop off of $\Sigma/\Sigma^{\text{id}}$ with density eventually coincides with the residual free energy of the untethered hard sphere fluid (black dashed line in Fig. 8). This corresponds to the expectation that the fraction of pores on a surface of a porous material is approximately equal to the pore volume fraction when the same size is sufficiently large. For intermediate values of the tether length, the value of $\Sigma/\Sigma^{\text{id}}$ falls below the residual free energy of the fluid

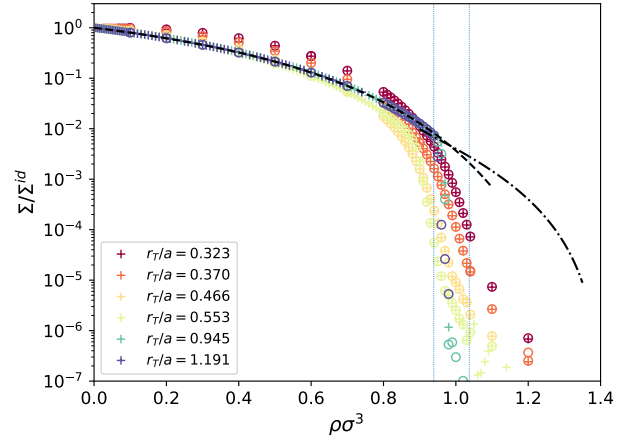


FIG. 8. Variation of the ratio of accessible tether bound phase space surface area with density at different fixed value of the tether length r_T/a . The pluses denote values calculated using $\Delta S_T^{(\sigma)}$, and the circles denote values calculated using $\Delta S_T^{(r_T)}$. The black dashed line is the residual free energy of the untethered hard sphere fluid¹³, and the black dashed-dotted line is the residual free energy of the untethered hard sphere FCC solid¹⁴.

at higher densities. These tether lengths correspond to those where there is a bottleneck in passing from the FCC to the disordered fluid regions of phase space (e.g., see $\rho\sigma^3 = 0.96$ in Fig. 7).

For all tether lengths, $\Sigma/\Sigma^{\text{id}}$ lie below the residual free energy of the untethered fluid at densities beyond the freezing density, eventually falling to zero. This is an indication that the system becomes trapped in the region of phase space near the FCC configuration.

VI. DIAGRAM OF STATES

If the entropy were an analytic function of the tether length r_T/a and the density $\rho\sigma^3$ for all state points, then the value of a line integral along any closed path should be zero. This implies that the entropy calculated by any path should lead to the same value. However, from the analysis of the entropy derived from the collision rates in Sec. IV, it is observed that this is not the case for the tethered hard sphere system, as the entropy determined by integrating the tether collision rate with respect to the tether length, at constant density, (see Eq. (8)) can lead to a different result to that obtained by integrating the particle-particle collision rate with respect to the density (or hard sphere diameter), at fixed tether length (see Eq. (7)). This implies that there must be regions in the states of the tethered hard sphere system (i.e. particular values of r_T/a and $\rho\sigma^3$) where the entropy is not analytic.

It is well established that thermodynamic integration cannot be performed through a first-order phase transition. In particular, the integration of the pressure cannot be used directly through the freezing transition to determine the free energy of

the solid phase. This has led to the development of a variety of alternate methods to determine the free energy of the solid phase, such as the Einstein crystal method^{2,15}, self-referential methods^{16–18}, as well as the use of the single occupancy cell model,^{3–6} along with other methods. This non-analytic behavior of the untethered hard sphere system in the fluid-solid transition region is expected to extend to the tethered systems. In fact, indications of this are given by the sharp drop in the pressure with density for sufficiently large tether lengths (see Fig. 5).

The difference between the entropy calculated from tether integration and density integration is shown in Fig. 6. In Fig. 6(a), it is observed that the differences between the two methods vanish for densities below about the freezing density. At low tether lengths (where $r_T/a \lesssim 0.55$), the two methods lead to the same result across all densities. The consistency between the two methods suggests that the entropy is analytic in these regions. In fact, it might be expected that the entropy is analytic everywhere the pressures are consistent between the two methods (see Fig. 5).

As can be seen in Fig. 6, the entropies between the tether integration and the density integration methods differ at densities above the freezing density and $r_T/a \gtrsim 0.55$. In this region, difference between the two methods is independent of density, but depends on the tether length, becoming larger with increasing r_T/a . This observation is in-line with the fact that the two methods lead to the same value pressure in this region (see Fig. 5). This implies that for a set tether length, the density integration entropies can be shifted by an amount independent of the density to align the results with the entropy calculated by tether integration. In Fig. 6(b), the difference between $\Delta S_T^{(r_T)}/k_B$ and $\Delta S_T^{(\sigma)}/k_B$ at a fixed density is shown as a function of tether length. The dashed black line is the entropy difference between the ideal tether model and an ideal gas (see Eq. (10)). As the density of the system increases, the difference between the two calculated entropies appear to approach a common curve which is independent of density; this curve differs from zero at a tether length $r_T/a \approx 0.55$ and monotonically increases, asymptotically growing as $3 \ln(r_T/a)$ for very large tether lengths.

A schematic diagram of states for a hard sphere system tethered to an FCC lattice is shown in Fig. 9. The shaded, light blue area on the left side of the diagram denotes the ideal tether state, where the particles are too far apart to interact with each other. The dark gray shaded area gives an indication of the region where we presume that the entropy is not analytic, based on where the entropy and pressure calculations depend on the method of calculation (see Fig. 3 and 5). For an untethered hard sphere system, which is related to the limit $r_T \rightarrow \infty$, there is a fluid-solid coexistence region with a fluid density of $\rho_f \sigma^3 \approx 0.93890$ and the melting density $\rho_s \sigma^3 \approx 1.03715$ ⁸. The non-analytic behavior of the entropy might be expected to be related to this transition and to persist as the tether length decreases. The gray region appears to vanish below a critical tether length of about $r_T/a \approx 0.55$. Outside this gray area, the entropy should be analytic. This implies that if we take a line integral around any simply closed path in this region (which excludes enclosing any portion of

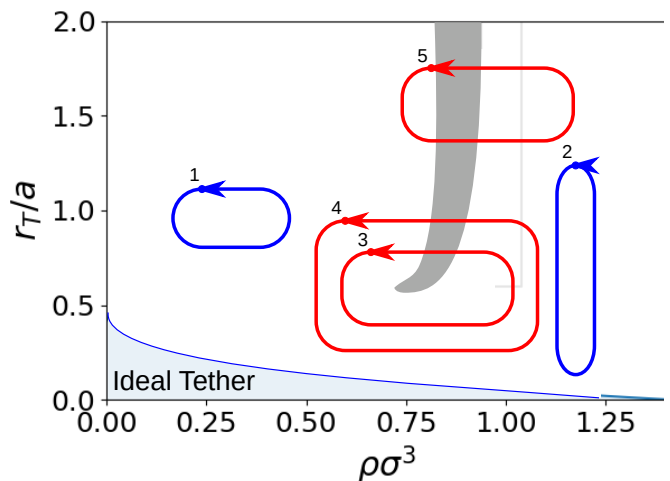


FIG. 9. Schematic diagram of states for tethered a hard sphere system. The blue shaded region denotes conditions where the system behaves as an ideal tether model. The dark gray shaded region is a qualitative depiction of the region where the entropy estimated to be non-analytic.

the gray shaded area) the results should be zero. For example, the line integral of the entropy along either of the blue curves would be zero.

If the line integral of the entropy encloses a portion of the gray shaded region, then its value would be non-zero. Examples of this include any of the red curves in Fig. 9 would be non-zero. Based on the observed differences in the excess entropies from tether integration and density integration, the value of the line integral would be positive, if the path is taken in a counterclockwise manner and negative if it is taken in a clockwise manner. The more of the gray region that is enclosed by the path, the larger the magnitude of the line integral; so the magnitude of the line integral for curve 4 would be larger than that for curve 3.

To attempt relate the non-analytical region of the entropy to structural changes of the system, the Steinhardt q_6 order parameter¹⁹ is calculated using the software package Freud²⁰, and the result is given in Fig. 10.

The Steinhardt order parameter characterizes the local organization of particles in the system. The directions of the “bond” vectors \mathbf{b} formed between a tagged particle and its nearest neighbors are projected along a set of spherical harmonic functions Y_{lm} of a particular order l :

$$Q_{lm}(\mathbf{b}) = Y_{lm}(\theta(\mathbf{b}), \phi(\mathbf{b}))$$

where \mathbf{b} is a “bond” vector. This quantity is then averaged over all bonds in the system to give $\langle Q_{lm} \rangle$. The Steinhardt q_l order parameter is defined¹⁹ as a rotationally invariant combination of these coefficients:

$$q_l = \left(\frac{4\pi}{2l+1} \sum_{m=-l}^l |\langle Q_{lm} \rangle|^2 \right)^{1/2}$$

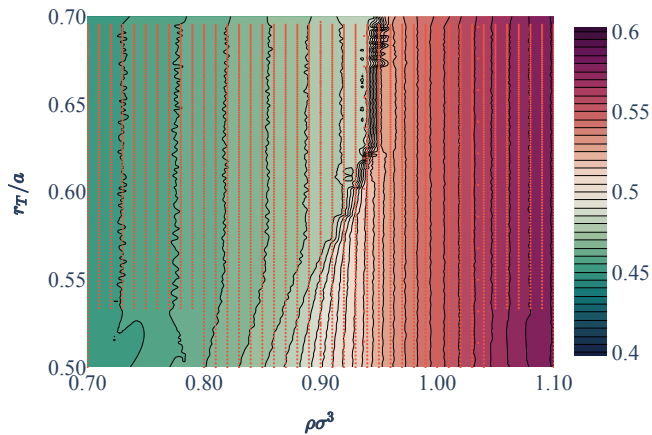


FIG. 10. A contour plot of the Steinhardt order parameter for the tethered hard sphere system in the vicinity of the analytic to non-analytic entropy transition. The value of the contours is indicated using the colour map on the right side. The small orange circles denote the state points where MD simulations are performed. The rapid change of the order parameter is indicative of a phase transition; however, the tethered system always retains some signature of its underlying tether lattice.

In this work, the value $l = 6$ is used as it is a good discriminator between FCC and random/fluid ordering.

The non-analytic region appears to correlate to where the order parameter rapidly changes, indicating the transition from a slightly less ordered structure held together by the tether at lower densities to a slightly more ordered structure at higher densities. Interestingly, there is an angled shape of the non-analytical region to below even the fluid transition density for the untethered system. It appears that staying below a tether length of $r_T/a \approx 0.55$ allows the avoidance of the non-analytic region entirely while performing thermodynamic integrations with respect to density. Previous uses of the tether model to calculate the free energy have been largely limited to integration with respect to the tether length, mainly to avoid the need to pass through the fluid-solid phase transition^{7,21,22}. Consequently, they did not consider the possibility of a continuous path between the fluid and solid phases which avoids the non-analytical region. Earlier works with the single occupancy model for hard sphere, where the particles are confined to Voronoi cells of the lattice sites, have used density integration to determine the free energy⁴; however, closer examination of the pressure variation with density indicated that these simulations did pass through a non-analytical region, although its effect was thought to be negligible.

VII. DISCUSSIONS AND CONCLUSIONS

In this work, the properties of systems of hard spheres that are tethered to an FCC lattice are examined. The tethered hard sphere model gives us detailed information of the structure of phase space, and more specifically the behavior of the entropy, around the point where the configuration is tethered. The

phase space of the system can be considered to be a porous material, with the pores corresponding to the regions accessible to the system, and the pore walls corresponding to the disallowed regions to overlap of spheres or violation of the tether constraint. The “pore volume” of phase space is directly related to the entropy of the system, while its “porosity” is directly related to the excess entropy of the system. The collision rates of the particles with their tethers give an indication of the pathways away from the perfect FCC configuration, while the collision rates of the particles with each other.

At low to moderate fluid densities, the porosity of phase space appears to be fairly uniform moving away from the perfect FCC configuration to the regions of phase space corresponding to the more disordered fluid phase. The tether collision rates gradually decrease to eventually reach the value for the ideal tether mode, while the particle-particle collision rates gradually increase from zero to the bulk fluid value.

At the higher solid densities, the FCC configuration becomes isolated from the rest of the phase space by excluded volume interactions. The system becomes “trapped” in the FCC configuration. Moving away from the perfect FCC lattice (by increasing the tether length), the particle-particle collision rate increases from zero to the values for the bulk, untethered system; however, the tether collision rate decreases exponentially with the tether length and then suddenly drops to zero.

At intermediate densities, there is a “bottleneck” separating the phase space corresponding to the FCC configuration and that of the disordered, fluid phase. The tether collision rate drops rapidly to low values as the tether length increases, before jumping up to the ideal tether rate. The particle-particle collision rate first increases to a value corresponding solid phase, but then later switches to the fluid phase value, sometimes transitioning back and forth between the two before settling to the fluid value.

This change in the pathways out of the FCC configuration leads to the entropy developing a path dependence, and this can be represented as a region in r_T/a and $\rho\sigma^3$ where the entropy is non-analytic. This region extends at extremely large tether lengths from the solid-fluid coexistence region of the untethered hard sphere system and ends at a tether length $r_T/a \approx 0.55$ and a density slightly lower than the density at the onset of freezing.

The direct geometric interpretation of the tether and particle-particle collision rates can be used to determine the entropy of the system: by integrating the particle-particle collision rate with respect to the system density or by integrating the tether collision rate with respect to the tether length. As long as both these paths do not cross this non-analytic region, they will lead to consistent results. If either path does cross the non-analytic region, then the discrepancy between the two methods will depend on what portion of the non-analytic region is enclosed by the path.

The results of this work can be extended in many ways. An FCC lattice is explored here; however, the particular shape of the non-analytic region is expected to depend on the lattice used for the tethers. For example, if the spheres were tethered

to a BCC (Body-Centered Cubic) lattice, then the location of the non-analytic region would be expected to change due to the difference in the fluid-solid coexistence densities as compared to the FCC crystal structure. A more interesting case is for a system that is tethered to a “fluid” configuration, rather than to a regular lattice. This would allow the behavior of particle systems that are trapped in glassy states to be explored. In fact, Speedy⁶ used this approach to calculate entropy of hard sphere systems that were jammed in various disordered configurations in order to determine the “statistical” entropy of the glassy system. It would be interesting to determine if the non-analytic region appears for these systems, if so, then where is it located, how does this depend on the particular arrangement of the tether sites, and how does this relate to the presence of a glass transition?

Also of interest is the relationship of the tethered particle model to the random pinning glass model^{23,24}, where a fraction of particles are forced to maintain a fixed position. The “pinning” of these particles imposes a quenched disorder in the system, which can be analyzed within the framework of the Random First Order Transition theory^{25–27}, and a glass transition is expected to occur, signaled by the vanishing of the configurational entropy, as the fraction of pinned particles increases above a critical value²⁷. Can the quenched disorder imposed by the tether constraint be analyzed in a similar manner?

The solid-fluid phase transition in the three dimensional hard sphere system is well established and understood. It would be interesting to examine the analytic structure of the entropy in the such as the two-dimensional hard disk system^{28,29} and the parallel hard cube model^{30–32}, where the transition has been more difficult to examine. After 65 years, there is still a rich variety of phenomena to explore in the phase transitions of hard systems, and the tether model opens a complementary line of investigation and interest.

¹B. J. Alder and T. E. Wainwright, *J. Chem. Phys.* **27**, 1208 (1957).

- ²D. Frenkel and B. Smit, *Understanding Molecular Simulation: From Algorithms to Applications*, 2nd ed. (Academic Press, San Diego, CA, USA, 2002).
- ³W. G. Hoover and F. H. Ree, *J. Chem. Phys.* **49**, 3609 (1968).
- ⁴L. V. Woodcock, *Faraday Discuss.* **106**, 325 (1997).
- ⁵L. V. Woodcock, *Nature* **385**, 141 (1997).
- ⁶R. J. Speedy, *Mol. Phys.* **80**, 1105 (1993).
- ⁷A. Donev, F. H. Stillinger, and S. Torquato, *J. Comput. Phys.* **225**, 509 (2007).
- ⁸C. Moir, L. Lue, and M. N. Bannerman, *J. Chem. Phys.* **155**, 064504 (2021).
- ⁹L. Lue, M. Bishop, and P. A. Whitlock, *J. Chem. Phys.* **155**, 144502 (2021).
- ¹⁰M. N. Bannerman, R. Sargant, and L. Lue, *J. Comput. Chem.* **32**, 3329 (2011).
- ¹¹L. Lue, *J. Chem. Phys.* **122**, 044513 (2005).
- ¹²M. N. Bannerman and L. Lue, *J. Chem. Phys.* **133**, 124506 (2010).
- ¹³N. F. Carnahan and K. E. Starling, *J. Chem. Phys.* **51**, 635 (1969).
- ¹⁴S. Pieprzyk, M. N. Bannerman, C. B. Arkadiusz, M. Chudak, and D. M. Heyes, *Phys. Chem. Chem. Phys.* **21**, 6886 (2019).
- ¹⁵D. Frenkel and A. J. C. Ladd, *J. Chem. Phys.* **81**, 3188 (1984).
- ¹⁶M. B. Sweatman, *Phys. Rev. E* **72**, 016711 (2005).
- ¹⁷M. B. Sweatman, A. A. Atamas, and J.-M. Leyssale, *J. Chem. Phys.* **128**, 064102 (2008).
- ¹⁸M. B. Sweatman, A. A. Atamas, and J.-M. Leyssale, *J. Chem. Phys.* **130**, 024101 (2009).
- ¹⁹P. J. Steinhardt, D. R. Nelson, and M. Ronchetti, *Phys. Rev. B* **28**, 784 (1983).
- ²⁰V. Ramasubramani, B. D. Dice, E. S. Harper, M. P. Spellings, J. A. Anderson, and S. C. Glotzer, *Comput. Phys. Commun.* **254**, 107275 (2020).
- ²¹R. J. Speedy, *J. Phys. Condens. Matter* **10**, 4387 (1998).
- ²²M. B. Sweatman, *Mol. Phys.* **113**, 1206 (2015).
- ²³S. Karmakar and G. Parisi, *PNAS* **110**, 2752 (2013).
- ²⁴S. Chakrabarty, S. Karmakar, and C. Dasgupta, *Sci. Rep.* **5**, 12577 (2015).
- ²⁵T. R. Kirkpatrick, D. Thirumalai, and P. G. Wolynes, *Phys. Rev. A* **40**, 1045 (1989).
- ²⁶V. Lubchenko and P. G. Wolynes, *Annu. Rev. Phys. Chem.* **58**, 235 (2007).
- ²⁷C. Cammarota and G. Biroli, *PNAS* **109**, 8850 (2012).
- ²⁸B. J. Alder and T. E. Wainwright, *Phys. Rev.* **127**, 359 (1962).
- ²⁹C. H. Mak, *Phys. Rev. E* **73**, 065104 (2006).
- ³⁰W. G. Hoover, *J. Chem. Phys.* **40**, 937 (1964).
- ³¹B. Groh and B. Mulder, *J. Chem. Phys.* **114**, 3653 (2001).
- ³²M. Marechal, U. Zimmermann, and H. Löwen, *J. Chem. Phys.* **136**, 144506 (2012).